The MICROSCOPE experiment, ready for the in-orbit test of the equivalence principle

P Touboul[1], G Métris[2], V Lebat[1] and A Robert[3]

[1] Onera, The French Aerospace Lab, F-91123 Palaiseau, France
[2] Université de Nice Sophia-Antipolis, CNRS (UMR 6526), Observatoire de la Côte d'Azur, Géoazur, F-06130 Grasse, France
[3] Cnes, F-31100 Toulouse, France

E-mail: pierre.touboul@onera.fr

Abstract

Deviations from standard general relativity are being intensively tested in various aspects. The MICROSCOPE space mission, which has recently been approved to be launched in 2016, aims at testing the universality of free fall with an accuracy better than 10^{-15}. The instrument has been developed and most of the sub-systems have been tested to the level required for the detection of accelerations lower than one tenth of a femto-g. Two concentric test masses are electrostatically levitated inside the same silica structure and controlled on the same trajectory at better than 0.1 Å. Any dissymmetry in the measured electrostatic pressures shall be analysed with respect to the Earth's gravity field. The nearly 300 kg heavy dedicated satellite is defined to provide a very steady environment to the experiment and a fine control of its attitude and of its drag-free motion along the orbit. Both the evaluations of the performance of the instrument and the satellite demonstrate the expected test accuracy. The detailed description of the experiment and the major driving parameters of the instrument, the satellite and the data processing are provided in this paper.

PACS number: 04.80.Cc

(Some figures may appear in colour only in the online journal)

1. Mission motivations

When developing his new theory of general relativity (GR), Albert Einstein devised three experiments to test some of its tiny consequences: the advance of Mercury perihelion, the deflection of the light by the Sun and the gravitational redshift of light [1]. Two of them were quickly verified: the expected GR deviation on Mercury precession rate, calculated by Einstein, corresponded almost exactly to the observed effect, unexplained by Newtonian gravity laws; Eddington verified during the 1919 total solar eclipse that light from stars was deflected due to the Sun mass by an angle corresponding to the GR prediction (which is twice the

Newtonian value) [2]. Gravitational redshift was first measured through the Pound–Rebka experiment in the 1960s with the change of gamma-ray wavelength at different al.

Space missions have provided in the last decade more accurate confirmations of the GR predictions. With the precise observation of the LAGEOS satellite orbital plane, taking into account Earth's gravity field models from the GRACE mission [3], the Lense–Thirring (or frame dragging) effect has been confirmed with 5% accuracy. Geodetic and frame dragging effects have been verified with cryogenic gyroscopes on-board GPB, a drag-free satellite [4]. Parameterized post-Newtonian (PPN) formalism helps to compare the accuracy of the performed tests of GR effects for the weak field [5]. The lunar laser ranging (LLR) leads to an estimation of the PPN parameter β with an accuracy of 1.1×10^{-4} thanks to the reflectors laid on the Moon [6]. The tracking of the Cassini spacecraft during its cruise from Jupiter to Saturn including a solar conjunction leads to an accuracy of 2.3×10^{-5} on the γ parameter [7]. Other space projects like the ACES mission are in preparation: one of its objectives is to perform in 2014 the time distribution and comparison between the in-orbit cold atom clock PHARAO, on board the International Space Station, with the ground clocks, and with a 10^{-16} accuracy; this leads to the possibility of redshift measurement up to a relative accuracy of 2×10^{-6} [8].

Nevertheless, GR remains a metric theory while other interactions are depicted in the standard model through a field theory in the rigid spacetime of special relativity. So testing the weak equivalence principle (WEP) not only tests the foundation of GR but also non-metric theories. Most string theories envisage this EP violation, introducing in particular additional fields such as the scalar field dilaton for instance [9]. Just as the search for the Higgs bosons at Cern aims to validate a prediction of the standard model, so the very accurate WEP test envisaged by the MICROSCOPE space mission may validate GR: both pave the way to new physics. Both experiments relate to supersymmetry, quantum gravity, or dark energy or dark matter.

After many years dedicated to the definition of the satellite and the systems, and to the development of the instrument, the MICROSCOPE mission has now been decided by Cnes and the launch is programmed in 2016. The whole in-orbit test conditions, the experimental apparatus and the procedures are now defined and specified to reach an accuracy of better than 10^{-15}. This is more than two orders of magnitude better than the test performed on ground with torsion balance pendulum [10]. This requires new techniques for the satellite and the payload, as well as a fine frequency analysis of the obtained signals to be corrected during the data processing. This mission also opens the way to even more ambitious ones that shall take advantage of the demonstrated approach.

2. Space experiment approach

The direct corollary of the WEP is the universality of free fall (UFF). Successful improvements and results of the WEP laboratory experiments have been obtained during the two last decades by the Eöt–Wash group with different materials such as Be, Al, Ti, Cu and Si [11]. In the same time, satellite experiments have been proposed to go further. The cryogenic STEP experiment proposed by Worden was the first one [12]; it has envisaged, more recently, EP test accuracy up to 10^{-18} with superconductive 2 K accelerometers and four pairs of test masses [13]. MICROSCOPE prepares these ambitious future missions performing a similar space test of UFF, by taking advantage of the existing micro satellite line in Cnes French Agency, but with a payload mass limited to less than 40 kg. The simple experiment of the test of the UFF would be the perfect comparison of the free fall of two masses in the same significant gravity field

over a long time span, with very weak perturbations with respect to this field. In practise, one part is almost achieved in the LLR experiment which compares the Earth and the Moon, freely falling in the gravity field of the Sun, in a very quiet environment [14, 15].

The MICROSCOPE aims at doing much better by using the gravity in the vicinity of the Earth which is roughly 1000 times larger than Sun's gravity and by measuring the position of two test masses with a much better accuracy than the accuracy of the laser ranging (about 10^{-11} m Hz$^{1/2}$ for the MICROSCOPE compared to about 1 cm for the LLR). But an ideal experiment could be killed by unwanted effects and it would be unrealistic to mimic the LLR experiment between two test masses orbiting the Earth for at least two reasons: the possible difference in free fall would be masked by non-gravitational effects on one hand and by gravity gradient effects on the other.

To overcome these drawbacks, the MICROSCOPE experiment controls the relative motion of the masses, which limits in particular the gravity gradient effects, inside the satellite forming a shield to the non-gravitational perturbations. More precisely, the electrostatic forces necessary to counteract the other accelerations are measured; they keep the two concentric cylindrical test masses on the same orbit. This is the principle of the differential accelerometer.

The difference of the gravitational accelerations between the two masses separated by the off centring $\vec{\Delta}$ is

$$\Delta \vec{\Gamma} = \vec{\Gamma}_1 - \vec{\Gamma}_2 = \delta_{12}\tilde{g} + [T]\,\vec{\Delta},$$

where $\tilde{g}$ is the gravity acceleration vector and $[T]$ is the gravity gradient tensor; δ_{12} is the Eötvös parameter measuring the difference of the ratios between the gravitational mass m_g and the inertial mass m_i for bodies 1 and 2:

$$\delta_{12} = 2\frac{\dfrac{m_{g1}}{m_{i1}} - \dfrac{m_{g2}}{m_{i2}}}{\dfrac{m_{g1}}{m_{i1}} + \dfrac{m_{g2}}{m_{i2}}} \approx \frac{m_{g1}}{m_{i1}} - \frac{m_{g2}}{m_{i2}}$$

The components of the monopole part of the gravity acceleration—more complete models are actually used but this does not modify the forthcoming analysis [16]—are expressed in a quasi-inertial frame, linked to the mean orbital plane and with Y being the orthogonal axis to the orbital plane, by

$$g_x = a\omega^2[\cos\theta + 2e\cos(2\theta + \varphi) + O(e)]$$
$$g_y = 0$$
$$g_z = -a\omega^2[\sin\theta + 2e\sin(2\theta + \varphi) + O(e)],$$

where ω is the orbital angular frequency, a and e are the semi-major axis and the eccentricity of the orbit, θ varies linearly with an angular frequency equal to ω and φ is a constant phase. As $e \ll 1$, the main part of the signal due to an EP violation is a periodic signal of angular frequency $\omega_{\mathrm{EP}} = \omega$ and amplitude $\delta_{12}a\omega^2$. The components of the gravity gradient are as follows:

$$T_{xx} = \tfrac{1}{2}\omega^2\left[1 + 3\cos(2\theta) + e\left(-\tfrac{3}{2}\cos(\theta-\varphi) + 3\cos(\theta+\varphi) + \tfrac{21}{2}\cos(3\theta+\varphi)\right) + O(e)\right]$$
$$T_{xy} = 0$$
$$T_{xz} = \tfrac{1}{2}\omega^2\left[-3\sin(2\theta) + e\left(\tfrac{3}{2}\sin(\theta-\varphi) - \tfrac{21}{2}\sin(3\theta+\varphi)\right) + O(e)\right]$$
$$T_{yy} = -\omega^2\left[1 + 3e\cos(\theta+\varphi) + O(e)\right]$$
$$T_{yz} = 0$$
$$T_{zz} = \tfrac{1}{2}\omega^2\left[1 - 3\cos(2\theta) + e\left(\tfrac{3}{2}\cos(\theta-\varphi) + 3\cos(\theta+\varphi) - \tfrac{21}{2}\cos(3\theta+\varphi)\right) + O(e)\right].$$

Note that T_{xy} and T_{yz} are null due to the fact that the X- and Y-axes are parallel to the orbital plane. Actually, this is valid up to a certain limit which is taken into account, but

this simplified formulation is adopted here for clarity of the analysis. As far as $e \ll 1$, the dominant part of the gravity gradient is at DC and at the $2\,\omega$ angular frequency; however, there are smaller terms of angular frequency $\omega = \omega_{EP}$. The measurement is optimized so as to obtain a larger sensitivity along the axis of the cylinders which will be the X-axis. On this axis, the difference of the gravitational acceleration between the two test masses will be

$$\Delta \Gamma_x = a\omega^2 \left(\delta - \frac{3e}{4a} (\Delta_x \cos \varphi + \Delta_z \sin \varphi) \right) \cos \theta + \frac{\omega^2}{2} \Delta_x$$
$$+ 3 \frac{\omega^2}{2} (\Delta_x \cos 2\theta - \Delta_z \sin 2\theta) + \text{small terms}.$$

The perturbing term $\frac{3e}{4a} (\Delta_x \cos \varphi + \Delta_z \sin \varphi)$ due to the gravity gradient is fully correlated with the EP signal and must be minimized. To this aim, the orbital eccentricity e and the off centring must be as small as possible, while the semi-major axis a must be sufficiently large. The semi-major axis is also subject to other constraints, one of them being to keep strong enough the gravity acceleration; it will be about 7100 km for the MICROSCOPE. By taking into account the injection errors and the perturbations of the orbit, the eccentricity, that the launcher should reach, is specified less than 5×10^{-3}. Under these conditions, each off centring Δ_x and Δ_z should be smaller than 0.1 μm to obtain a perturbing term much smaller than the eventual EP violation signal, 10^{-15} times the field. Taking into account that the off centring between the two test masses is the result of a complex assembly, the specification of 0.1 μm is not reachable directly, even with very sophisticated manufacturing procedures and accurate electronics. The off centrings Δ_x and Δ_z are expected to be less than 20 μm after the instrument manufacturing and integration. So they shall be estimated in flight with 0.1 μm accuracy, thanks to the large gravity gradient signal of amplitude $3\frac{\omega^2}{2a}\Delta$ at the angular frequency 2ω. Then, their effects will be corrected in the ground data processing with an accurate Earth's gravity field model [16]. This requires the knowledge of

- the absolute dating of the measurements with an accuracy of 50 ms,
- the satellite position with an accuracy of 7 m at the f_{EP} frequency and
- the instrument pointing with accuracies from 3 μrd to 2.5 mrd depending on the frequency.

The first two specifications are not very stringent considering the standard state of the art, but the third is challenging and has required the development of specific procedures including a hybridization between the angular measurements delivered by the star sensors and the angular accelerations measured by the on-board accelerometers.

In the previous paragraphs, we have considered the satellite and the test masses inside, with no rotation with respect to the quasi-inertial frame. A rotation around the Y-axis, keeping X and Z parallel to the orbital plane, can also be considered with a constant spin rate (see figure 1). Then, the projected gravity acceleration varies in the instrument frame with a frequency $f_{EP} = f_{orb} + f_{spin}$. The gravity gradient has also a modified spectral representation and has no longer a contribution at f_{EP} frequency. The spinning mode has other advantages like, for instance, reduced thermal perturbations at f_{EP} frequency, larger than f_{orb}. Nevertheless, more stringent requirements on the angular stability must be met in the spinning mode than in the quasi-inertial mode. To take advantage of the different configurations, MICROSCOPE will operate sequentially either in the quasi-inertial mode or in the spinning mode with two different frequencies, f_{spin}, so that $3f_{orb} < f_{spin} < 5f_{orb}$.
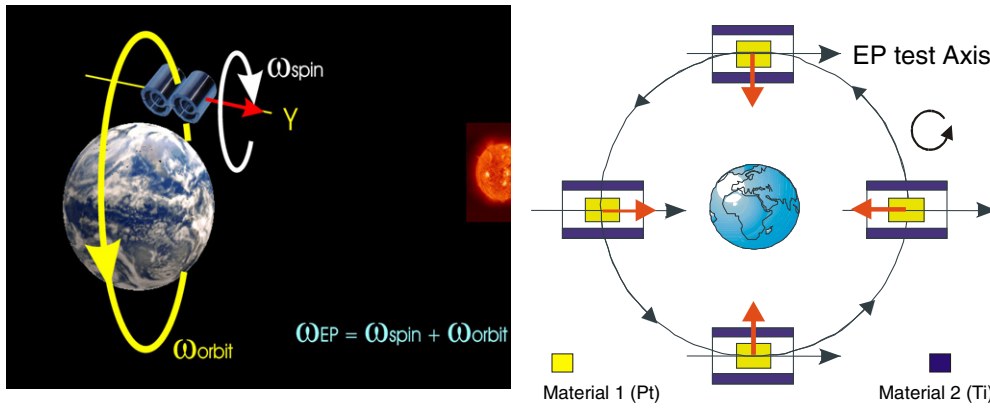
Figure 1. Configuration of the experiment: the Sun is in the direction normal to the orbital plane and the satellite rotates about this normal axis; Earth's gravity is modulated in the instrument reference frame (in black) by this rotation; the EP test is performed at 1.7×10^{-3} Hz orbital frequency in satellite inertial pointing and at about 10^{-3} Hz when the satellite is spinning.

For the success of the experiment, the test masses must react in the same way to the same source of gravity in the absence of EP violation. As far as the Earth's gravity is concerned, the test masses can be considered as point masses due to the large distance from the source and the centring condition is sufficient. The local gravity due to the satellite is mainly at DC and is thus uncorrelated with the EP signal, but care is taken for small variations at f_{EP} due to thermo-elastic behaviour of the satellite and of the instrument structure. The effects can be reduced to an acceptable level when the cylindrical masses behave like homogeneous spheres up to the second order of the momentums of inertia (i.e. the matrix of inertia is proportional to the identity matrix). This condition also allows reducing the gravity torque acting on the masses which are used as references to measure the angular acceleration of the satellite. The applied electrostatic torques, used to counteract, are then quite proportional to the angular acceleration of the satellite.

The MICROSCOPE encloses two differential accelerometers, 171 mm apart along the Y-axis. One differential accelerometer will compare the free fall of two test masses made of the same material. This provides a very strong check of the experiment, allowing the estimation of the part of the signal which is due to experimental limitations and systematic errors. The second differential accelerometer will compare the free fall of a test mass made in platinum and titanium. The choice of these two materials is the result of a trade-off between the scientific interests regarding the EP test, theoretical properties [17], macroscopic properties (concerning magnetic susceptibility, chemical stability, off gassing, thermal expansion, conductivity, etc) and manufacturing compliance.

The MICROSCOPE experiment requires at the same level the best accuracy and the control of the exactitude of the results. That is why many sessions are dedicated to the control of the satellite, the verification of the instrument operation and the sensors calibration. By finely controlling the satellite cinematic motion, calibrated acceleration field can be applied to the masses and observe by the sensors [18]. In the same spirit, a balance between performing multiple sessions dedicated to the EP test under various conditions (various spin rates, various positions of the test masses, etc) and having a few longer sessions in order to improve the signal to noise ratio has been established. The adopted trade-off remains on different sessions of 120 orbital periods. This is long enough to obtain the Eötvös parameter target exactitude
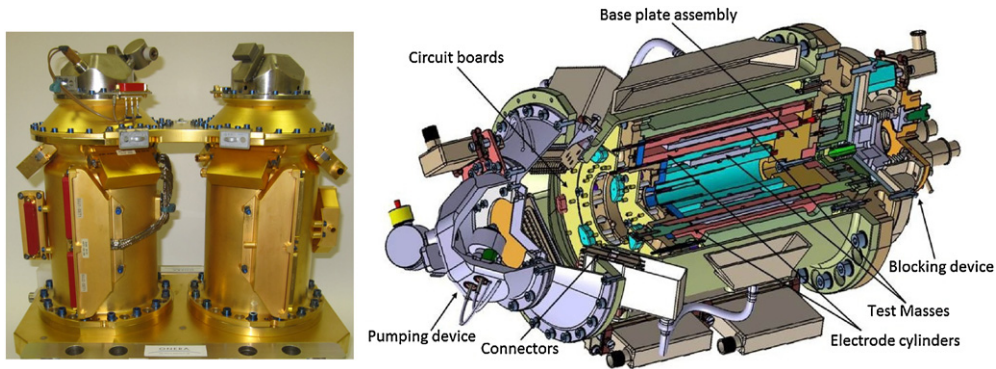
Figure 2. T-SAGE gold-coated tight housings including two concentric inertial sensors (left); cutaway view of the concentric sensors with the two test masses—in violet—surrounded each by two silica electrode cylinders—in red—(right).

of 10^{-15} in inertial mode and even better in rotating mode, by reducing the stochastic error with respect to the systematic evaluated one. This is also short enough to have time for many sessions with different experimental conditions.

3. The experimental technique

The electrostatic differential accelerometer, called twin space accelerometer for gravitation experiment (T-SAGE), is derived from previous developed instrument carried on board the GRACE [19] and GOCE satellites [20]. The MICROSCOPE payload case can only embark two identical instruments whose mechanical cores are fixed on the same rigid interface structure (see figure 2). Each accelerometer is composed of two concentric inertial sensors integrating, respectively, the inner and the outer test masses.

The cylindrical test masses are made, respectively, of platinum rhodium and titanium alloys for the first accelerometer and only platinum rhodium for the second one which is a reference instrument to calibrate the systematic and stochastic errors and the limitations of the experiment procedures. The test is then based on a double difference, dissymmetry of actuations on the masses of different composition and difference with the reference test masses made of the same material. Cyclic conditions on the mass composition were selected for other missions considering a larger payload with four pairs of masses and three different materials [21].

Identical test mass shapes and not mass values have been chosen in the design because the operation of the instrument is based on capacitive position sensing and electrostatic actuation; both are only dependent on the geometry of the configuration of perfect electrostatic conductors. Each test mass is servo-controlled motionless with respect to the instrument frame, so the mass value is only a loop parameter which does not fix directly the instrument response like in passive mass–spring devices.

The masses of the qualification model (QM), as well as of the flight models (FMs), have been produced by PTB in Germany, requiring dedicated machining processes to reach the absolute sizes of the geometry with an overall defect of less than 3 μm (leading to less than 7×10^{-4} relative dissymmetry of momentum of inertia). The conicity is less than 3.5×10^{-5} rd for the smaller mass and 2×10^{-5} rd for the larger one, limiting the coupling between the radial motion control and the axial one, on which the EP test is performed: moreover, radial

electrostatic stiffness and fluctuations of electrostatic bias force are weakly projected on the radial direction. Each mass also features four flat areas on its external face, breaking the symmetry of revolution and thus allowing performing the measurement and control of the mass axial spin. They have been defined and specified to preserve the equality of the moments of inertia with the needed accuracy. In addition, three conic holes, machined on each edge face, fit with two sets of three fingers used to block the mass during the launch vibrations. A pneumatic device integrated under the sensor core allows freeing the mass in orbit by removing one set of 150 μm: the 45° cones limit the mass motion to ± 75 μm in all directions.

Each test mass is surrounded by two gold coated cylinders made of silica Suprasil II, exhibiting a 1.5×10^{-7} coefficient of thermal expansion at 25 °C. Associated with the 1 mK thermal stability of the instrument interfaces, it ensures a very steady set of electrical conductors around the mass. On the inner cylinder, four pairs of electrodes are engraved for the control of the four radial degrees of freedom (two translations and two rotations). On the outer cylinder, the electrodes are used to control both the axial direction and the spin around this axis. The cylindricity and the coaxiality of the cylinders, as well as the geometry of the electrodes, are mandatory for performing the electrostatic levitation of the mass in the right position and attitude. Dedicated machining has been developed by abrasive ultrasonic grinding leading to 2 μm geometry accuracy. So, the present integration of the QM instrument leads to masses off centring smaller than 4 μm along the revolution axis and smaller than 12.3 μm in the radial directions; moreover, the axial directions of both sensors are aligned with 3.25×10^{-4} rad accuracy.

The four cylinders of the two inertial sensors are actually integrated on a unique silica centring part. They are clamped with a semi-rigid inner housing on an invar sole plate, also accurately machined (within 5 μm) and serving as a reference frame for the sensors (see figure 2). Feedthroughs in this plate link the masses and the electrodes to the electronics units; associated with the tight housing, they allow the sensor operation in a 10^{-5} Pa vacuum, reducing the radiometer effect on the mass and the gas Nyquist fluctuation dissipation [22].

This housing includes on its top a pumping device and a getter for vacuum management, and under the sole plate a blocking mechanism of the two masses. It is gold coated for thermal insulation and stability, taking advantage of the very weak and steady power consumption inside the housing due to the inertial sensor capacitive operation. It also constitutes a fine electrical shielding against not only the spacecraft sub-systems electrical fields but also against the Lorentz forces induced by Earth's magnetic field.

The specific procedures for the integration have recently been controlled and assessed with fine metrology of the QM assembly before and after the vibration and thermal cycling tests. The repeatability of the mounting and dismounting of the parts confirms the obtained gaps between the radial and axial electrodes and the masses, i.e. respectively, for the inner sensor, 598–603 $\pm$ 1 μm and 598–601 $\pm$ 1 μm for the outer one; it also confirms the mass distance to the stops to 75 $\pm$ 10 μm and the mass off centring to less than 2 μm for the X-axis.

The 10^{-15} EP test performance requires the following characteristics for the inertial sensors:

(a) Free mass motion without force disturbances: radiometric effect, radiation pressure, off gassing, difference of contact potential and back actions from capacitive sensing pumping signals are smaller than the damping introduced by the 5 μm gold wire which links the mass to the electrical potential reference needed to preserve its charging by space proton fluxes; this stochastic disturbance is evaluated between 1.4×10^{-12} and 3.2×10^{-12} ms^{-2} Hz$^{-1/2}$ depending on the EP test frequency (orbital frequency or orbital frequency + spin frequency).

Table 1. Axial sensing and actuation performance verified on FM electronic unit.

Capacitive position sensing					
Mass	Capacitive sensor gain in V pF^{-1}	Resolution in F Hz$^{-1/2}$	Geometry factor in pF μm^{-1}	Position sensitivity in V m^{-1}	Resolution in m Hz$^{-1/2}$	Bias thermal sensitivity in m K^{-1}
Ti ext	40	2.5×10^{-19}	6.5	2.6×10^5	3.8×10^{-11}	24×10^{-11}
Pt int	80	1.25×10^{-19}	3.7	3.0×10^5	4.0×10^{-11}	4.5×10^{-11}
Electrostatic actuators					
Mass	Actuator gain in N V^{-1}	Electrical Noise in μV Hz$^{-1/2}$	Resolution in N Hz$^{-1/2}$		Maximum range in N	Bias thermal sensitivity in N K^{-1}
Ti ext	3.21×10^{-8}	0.15	4.8×10^{-15}		1.278×10^{-6}	6.4×10^{-14}
Pt int	1.86×10^{-8}	0.15	2.8×10^{-15}		0.740×10^{-6}	3.7×10^{-14}

(b) Six high performance servo-control channels for the mass control along the same orbit: the FM electronic units are currently tested; the obtained resolutions in position are presented in table 1 and lead to an axial acceleration of less than 6×10^{-17} ms^{-2} at f_{EP} ($\omega_{EP}^2 < 4 \times 10^{-5}$ and integration of the signal over 20 orbits) with the back action of the needed pumping signal, respectively, limited to 8.0×10^{-15} and 3.9×10^{-15} ms^{-2} Hz$^{-1/2}$; the drive voltage amplifiers, which control the charge injected on the electrodes to counteract any relative acceleration, are also verified in very good agreement with the EP test requirements and the demonstrated 10 mK thermal stability at f_{EP} of the electronics unit is sufficient for the related bias thermal sensitivities.

(c) Six digitalized outputs corresponding to the three linear and angular accelerations generated by the electrical field configuration and exhibiting high resolution and stability: limited couplings are obtained between the channels by the geometry of the masses and the electrode cylinders; selected pickup measurement circuits exhibit, at low frequencies, noise equivalent to levels of applied voltages on the electrodes of 4.5 μVHz$^{-1/2}$ for the Pt mass and 6.3 μVHz$^{-1/2}$ for the Ti one, corresponding, respectively, to 2.1×10^{-13} and 6.7×10^{-13} ms^{-2} Hz$^{-1/2}$.

The recent tests of the electronic unit, the control of the test mass geometry, the verification of the integration accuracy and the qualification phase of the instrument have assessed the expected intrinsic performance of the sensors. In addition, the satellite must provide the very soft environment needed for the experiment.

4. The experiment cocoon, the MICROSCOPE dedicated satellite

The MICROSCOPE mission is developed in the frame of scientific missions exploiting the CNES MYRIADE micro-satellite product line. But the 'unusual' MICROSCOPE mission requirements have several consequences on the satellite design.

First, the satellite shall protect the payload and thus the test masses from all non-gravitational forces perturbing the EP test experiment. So an active control of the acceleration and the attitude of the satellite is necessary. Indeed, the common acceleration of the spacecraft shall be less than 10^{-12} ms^{-2}, at EP test frequency, the angular pointing stability less than 7 μrad, the angular velocity stability less than 10^{-9} rad s^{-1} for the EP measurement sessions
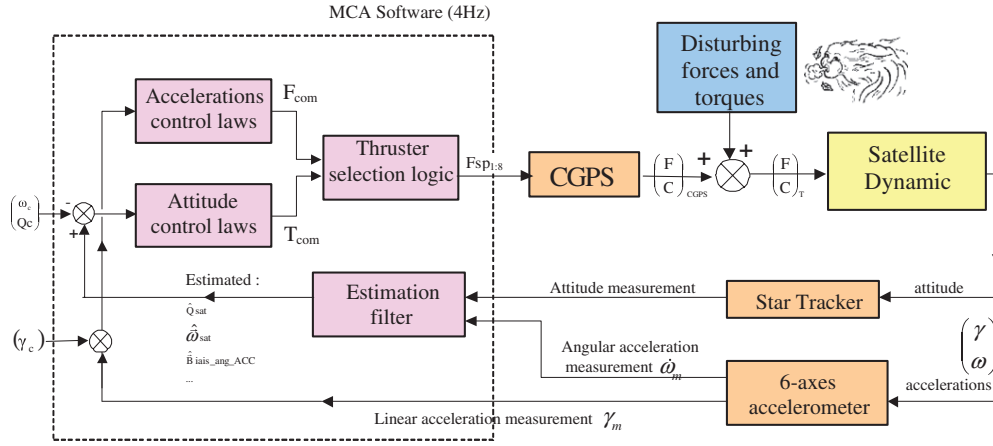
Figure 3. AACS control loop.

with a spinning satellite and the angular acceleration less than 10^{-11} rad s^{-2}. This specific function of the satellite, called acceleration and attitude control system (AACS), needs a very sensitive six-axis sensor and several very fine actuators.

Because of its outstanding sensitivity and in order to avoid a specific new development, T-SAGE itself is used as the main sensor of the AACS control loop. The controlled accelerations are directly provided by T-SAGE to AACS as the result of the combination of the accelerations measured by the proof masses corrected by the scale factor and the choice of a drag-free point. The estimated attitude is the result of the hybridization between the attitude measurements provided by the Star Trackers and the angular accelerations measured by T-SAGE.

The control laws for the acceleration and the attitude servo loops define the total forces F_{com} and torques T_{com} to be applied on the satellite to compensate the external perturbations; the selection logic transforms the commanded forces and torques into eight thrust orders sent to the cold gas propulsion system (CGPS). The control loop is shown in figure 3.

The CGPS is made of eight micro thrusters, distributed in pairs on four opposite corners of the satellite and using gaseous nitrogen as a propellant to produce the few micronewtons of thrust required by the AACS. Six tanks are symmetrically accommodated in order to avoid self-gravity disturbances on the masses (see figure 4). The thrusters take advantage of the development of the GAIA satellite and have recently been tested in a vacuum chamber with a dedicated thrust balance. The simulation of the system has demonstrated the possibility to implement a gain of more than 1000 in a narrow band around f_{EP} with less than 10^{-2} Hz width.

In addition, the required very stringent thermal stability of the payload highly constrains the spacecraft design. The stability of the sensors shall be better than 1 mK at f_{EP} for the mechanical core and 10 mK for the electronics units. So, a heliosynchronous orbit has been selected guaranteeing the Sun orientation stability and the maximum power for limited solar arrays. In addition, the thermal control of the payload and of the satellite is separated, both avoiding any active control to the benefit of the T-SAGE stability.

The payload is uncommonly accommodated at the centre of the spacecraft, whereas MYRIADE microsatellites usually have their payload on an external wall, in particular for
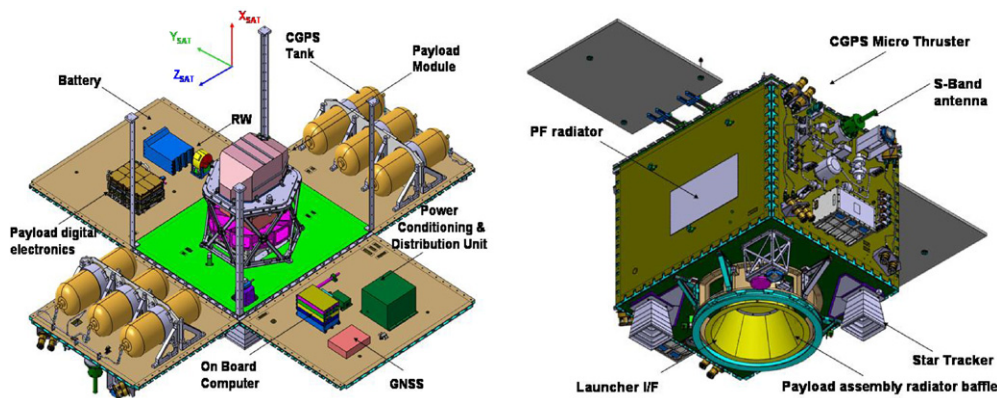
Figure 4. MICROSCOPE satellite internal layout (left) and external layout (right); note that the global navigation satellite system receiver is only optional.

optical and radar missions. The same internal case supports on its top the sensor housings and at the middle the electronics units. It also includes the thermal control hardware and provides the centring of the proof masses with respect to the satellite spin axis. It exhibits a very high mechanical stability during the entire mission. This guarantees the thermal operating range of 10–45 °C, taking into account the 6 W power dissipation of each electronic unit. Besides the thermal stability, it also includes a magnetic shielding for the masses. The thermal stability of each payload unit has been tested and has confirmed the two-stage insulation. The first stage supports the electronic units, thermally linked to the outer radiator, and insulated itself from the satellite structure by six titanium alloy blades. As shown in figure 1, this anti-Sun radiator is protected from Earth's albedo by a cone so that the thermal conditions do not vary. The second stage which supports the two housings and the magnetic shielding is mechanically linked and thermally insulated from the first stage by six titanium alloy blades.

Apart from the thermal effects, three categories of internal micro-perturbations have been considered and reduced in the satellite design: mechanical, gravitational and magnetic. Any mass displacement inside the spacecraft has been suppressed except the gas consumption and its thermo-elastic effects have been finely analysed. These modifications of the distribution of mass may also change the self-gravity gradients but these effects have been checked and are very weak at f_{EP}. The electrical activity of the circuits and the equipments of the satellite may change the internal magnetic field but the instrument shielding provides margins against these potential effects.

Some of these perturbations may be much stronger during the eclipse season (three months a year) at the transition of the satellite into Earth's shadow, inducing several phenomena: sudden solar pressure variation, MLI thermo elastic clank, non-regulated bus voltage variation, etc. For these reasons, the EP test is not performed during this period which may be used on the opposite to characterize the payload sensitivities to these increased perturbations.

5. Experimental and mission status

Recent decisions in Cnes have started the production of the satellite from the detailed definition established in very strong relationships with the instrument and the test procedures. The satellite is actually in a certain way the Einstein falling elevator in which the MICROSCOPE experiment

Table 2. Evaluation of the MICROSCOPE space experiment performance: four major sources.

Stochastic error sources	In ms^{-2} Hz$^{1/2}$	Systematic error sources at f_{EP}	In ms^{-2}
Accelerometer noise	1.36×10^{-12}	Pointing stability	4.8×10^{-16}
Centrifugal acceleration	0.30×10^{-12}	Magnetic field	4.0×10^{-16}
Angular acceleration	0.20×10^{-12}	Sensor thermal variations	3.5×10^{-16}
Sensor thermal gradient	0.19×10^{-12}	Drag-free residual acceleration	3.3×10^{-16}

is performed and the EP test accuracy depends not only on the instrument performance presented in section 3 but also on both the ways the common disturbances are rejected in the inertial sensor output difference and the sufficient limited levels of the differential disturbances.

The satellite angular and centrifugal accelerations have a limited impact in the observed difference of the measured accelerations thanks to both the satellite AACS and the mass centring. The evolution of the satellite attitude has been simulated taking into account the accuracy of the star sensor quaternion and of the angular accelerations delivered by the payload itself, as well as the resolution of the cold gas thrusters. These thrusters have been recently tested and qualified successfully for the GAIA mission satellite. As shown in table 2, the stochastic variations should not affect the test when compared with the instrument intrinsic noise. Systematic error may appear in the pointing stability of the satellite (necessary to reduce and correct the gravity gradient), because of artefact signals delivered by the pixels of the star sensor and of the thermo-elastic deformation of the satellite structure which carries the star sensors and the accelerometers. The evaluation of the differential acceleration due to the pointing fluctuations is provided in table 2.

The residual linear acceleration of the satellite on which both differential accelerometers are fixed is servo controlled through the drag compensation loop of the satellite. An acceleration residue may be applied to both masses and a difference of sensitivity or alignment of the two inertial sensors may introduce differences in the measured accelerations which depend on the matching accuracy of these instrument parameters.

Other differential accelerations may be applied on the test masses because of their difference of magnetic susceptibility and volume when considering the residue of the field and its gradient inside the payload shielding. Fluctuations of the temperature of the sensor and its thermal gradients modify, respectively, the gold wire stiffness and the radiometer and the radiation pressures applied on the test masses.

The corresponding contributions of the four major errors, depicted above and which limit the EP test accuracy, are provided in the case of a spinning satellite in table 2. In fact, hundreds of contributions at instrument or satellite levels have been evaluated from the specifications or the control measurements. They have been presented to the Cnes review committee and the specifications are followed in the present development phase of the satellite. They will be considered when in orbit according to the instrument and the experiment environment knowledge.

The quadratic sum of the stochastic and systematic errors leads presently to 1.5×10^{-12} ms^{-2} Hz$^{-1/2}$, dominated by the accelerometer noise and 1.1×10^{-15} ms^{-2} at f_{EP} corresponding to many sources at similar levels: a quadratic sum is performed because the worst case values of numerous independent systematic sources (and without correlated phase) are statistically considered. This is compatible to the 10^{-15} EP test accuracy and even better, considering the 8 ms^{-2} level of gravity at 720 km altitude. Because the experiment will be performed several times with steady conditions over a minimum of 20 orbits, predominant

stochastic errors should be reduced and several 10^{-16} accuracies obtained. Errors are larger when considering the inertial pointing of the satellite with lower f_{EP}, equal to the orbital frequency: thermodynamic noise is increased, thermal filtering is reduced, drift is larger, Earth's gravity gradient more disturbing. Measurement sessions of 120 orbits have been thus considered and 10^{-15} EP test accuracy should be obtained.

The GOCE satellite, launched in March 2009 at an altitude of 260 km, integrates six space electrostatic accelerometers which constitute the sensors of the on-board gravity gradiometer [23]. These instruments have been developed in our laboratory with the same concept and technology than the MICROSCOPE instrument, except the cylindrical concentric configuration. They have demonstrated, in orbit for now more than three years, that they can exhibit residual noise lower than 3.1×10^{-12} ms^{-2} Hz$^{-1/2}$. Many in-orbit tests corroborate the instrument models and error budgets. Concerning the stochastic errors, both instruments are in the same range. Concerning the frequency bandwidth, the GOCE accelerometer is more demanding because of a needed performance between 0.005 and 0.1 Hz while the MICROSCOPE performance must be reached at a very narrow frequency bandwidth around f_{EP}. Conversely, the MICROSCOPE experiment is much more demanding for the long-term stability of the instrument environment (thermal, magnetic, accelerometric, etc) that must be insured by the satellite.

The ground data processing which we have developed has already considered the needed frequency analysis and the limitation introduced by the limited duration of the measurement sessions. In addition, we have anticipated possible small lacks in the data series which may appear because of some difficulties of the satellite-ground telemeasure system. They could slightly modify the spectral characteristics of the signal. Furthermore, in-orbit calibration of the instrument will be performed by shaking the satellite along and about selected axes to compare the inertial sensor responses. A similar approach has been performed successfully in the GOCE mission. Corrections of the measurements have to be performed to compensate the differences of the response. So, the Onera-OCA's scientific mission centre will not only post-validate the data before the distribution and the archiving, but will also verify, in a week delay, the behaviour of the experiment so that the mission scenario can be modified if necessary. The 1.5-year mission duration, limited by the embarked quantity of propulsion gas, must be exploited very efficiently.

While the satellite will be integrated and tested during the next four years, free fall tests of the FM instrument will be performed, as already done for the QM in the ZARM drop tower in Bremen, Germany [24]. Electrostatic levitation of the mass (not possible in the laboratory due to the too-strong gravity acceleration) has been obtained during these free fall tests. Improvement of the capsule conditions as well as catapult operation for an up and down free motion is envisaged to optimize these tests. Indeed, during more than the first 2 s, vibrations of the capsule larger than 50 μms^{-2} are observed and the fall duration is limited to less than 4.8 s (see figure 5).

The launch of the satellite is envisaged in 2016 leaving time to pursue very fine characterization of the sensors in conjunction to the detailed verification of the sensor core and the electronics operation.

6. Perspectives

The MICROSCOPE mission is designed to test the identity of the free fall of two masses in platinum and titanium with an exactitude of 10^{-15}. This will bring a major constraint for any theory aiming at extending the Einstein theory of gravitation, whatever the result will be.
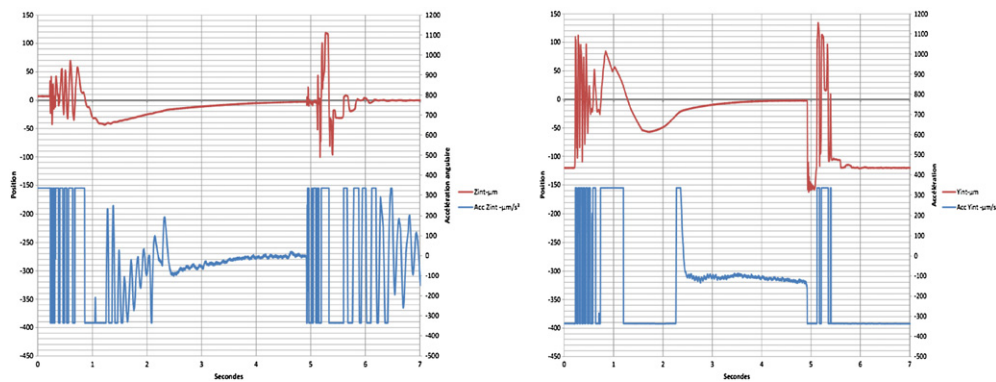
Figure 5. Mass electrostatic radial levitation: in red the mass position, in blue the electrostatic force, horizontal (left), vertical (right).

However, the practical consequences will be different in the case of a violation or not. If the experiment concludes to an EP violation, the subsequent actions to achieve should be

- To maximize the level of confidence about the result: this is already our spirit in the definition of the mission (an example is the test with two masses made of the same material) and the preparation of the data analysis, but this will be reinforced by numerous and independent cross checking; the stronger confirmation would be an independent experiment.
- To duplicate the MICROSCOPE experiment with only marginal modifications, but with test masses made of other materials; numerous studies and developments would be recurrent and thus the cost of these missions would be much smaller than the cost of MICROSCOPE.
- To perform even more accurate experiments, taking advantage of the MICROSCOPE development, in view of determining all parameters that may be involved in this violation.

If MICROSCOPE shows the absence of EP violation at the 10^{-15} level, the next step will be logically to define a new experiment with a better accuracy. The knowledge issued from MICROSCOPE will be a fundamental heritage for these new missions. Besides its fundamental objective to test the equivalence principle, MICROSCOPE will additionally set up technological key points for future missions such as the acceleration and the attitude control system (an extension of the drag-free system).

Acknowledgments

References

[1] Einstein A 1916 *Ann. Phys., Lpz.* **49** 769–822
[2] Dyson F W, Eddington A S and Davidson C 1920 *Phil. Trans. R. Soc.* A **220** 291–333
[3] Tapley B 2005 *J. Geod.* **79** 467–78
[4] Everitt C W *et al* 2011 *Phys. Rev. Lett.* **106** 221101
[5] Will C M 1971 *Astrophys. J.* **163** 611–28
[6] Williams J G, Turyshev S G and Boggs D H 2004 *Phys. Rev. Lett.* **93** 261101

[7]   Bertotti B, Iess L and Tortora P 2003 *Nature* **425** 374–6
 [8]   Cacciapuoti L and Salomon C 2009 *Eur. Phys. J.* **172** 57–68
 [9]   Damour T and Donoghue J F 2010 *Class. Quantum Grav.* **27** 202001
[10]   Schlamminger S, Choi K Y, Wagner T A, Gundlach J H and Adelberger E G 2008 *Phys. Rev. Lett.* **100** 041101
[11]   Adelberger E G, Gundlach J H, Heckel B R, Hoedl S and Schlamminger S 2009 *Part. Nucl. Phys.* **62** 102
[12]   Worden P W Jr 1976 *PhD Thesis* Stanford University
[13]   Sumner T J 2007 *Adv. Space Res.* **39** 254–8
[14]   Nordtvedt K 1968 *Phys. Rev.* **170** 1186–7
[15]   Damour T and Vokrouhlicky D 1996 *Phys. Rev.* D **53** 4177–201
[16]   Bruinsma S, Lemoine J-M, Biancale R and Valès N 2010 *Adv. Space Res* **45** 587–601
[17]   Damour T and Blaser J-P 1994 *Particle Astrophysics, Atomic Physics and Gravitation* ed J Tran Thanh Van,
         G Fontaine and E Hinds (Gif-sur-Yvette: Editions Frontières) pp 433–40
[18]   Levy A, Touboul P, Rodrigues M, Metris G and Robert A 2010 *SF2A* ed S Boissier, M Heydari-Malayeri,
         R Samadi and D Valls-Gabaud pp 123–6
[19]   Flury J, Bettadpur S and Tapley B D 2008 *Adv. Space Res.* **42** 1414–23
[20]   Touboul P, Foulon B, Christophe B and Marque J P 2011 *Geodesy for Planet Earth* vol 136 ed S Kenyon *et al*
         (Berlin: Springer) pp 215–21
[21]   Mester J 2001 *Class. Quantum Grav.* **18** 2475–86
[22]   Touboul P 2010 *Space Science Series of ISSI* vol 34 ed C W F Everitt *et al* (New York: Springer) 507–26
[23]   Floberghagen R, Fehringer M, Lamarre D, Muzi D, Frommknecht B, Steiger C, Piñeiro J and da Costa A 2011
         J. Geod. **85** 749–58
[24]   Selig H, Dittus H and Lammerzahl C 2010 *Microgravity Sci. Technol.* **22** 539–49